Nationaal Lucht- en Ruimtevaartlaboratorium
National Aerospace Laboratory NLR

NLR-TP-2000-013

Numerical results of lifting surface theory

Cat. 4 Benchmark Problem 3rd CAA Workshop

J.B.H.M. Schulten and M. Namba

Nationaal Lucht- en Ruimtevaartlaboratorium
National Aerospace Laboratory NLR

NLR-TP-2000-013

Numerical results of lifting surface theory
Cat. 4 Benchmark Problem 3rd CAA Workshop

M. Namba* and J.B.H.M. Schulten

* Kumamoto Institute of Technology, Japan

This report is based on a presentation (to be) held on the Third Computational Aeroacoustics (CAA) Workshop on Benchmark Problems, Cleveland, Ohio, USA, November 8-10, 1999.

Division: Fluid Dynamics
Issued: 31 January 2000
Classification of title: Unclassified

Summary

This paper presents two lifting surface solutions of the Category 4 benchmark problem of the Third Computational Aeroacoustics (CAA) Workshop, held at Cleveland, Ohio, USA, 8-10 November, 1999. The problem studied is rotor-stator interaction noise for a generic configuration, described in appendix C. Although the boundary value problem is the same for both authors, there are quite some differences in their analytical modeling and subsequent numerical solution techniques. In general, the numerical results of both authors agree reasonably well. It appears that the agreement in vane pressure jump is very satisfactory.

Contents

(32 pages in total)

List of symbols

a_0	ambient speed of sound
B	number of rotor blades
h	hub radius
K	Kernel
$k_{m\mu}$	radial eigenvalue [Eq. 10]
M	Mach number
M_T	Ω
q	radial wake periodicity [App.C, Eq.2]
R	tip radius
r	radial coordinate
t	time
U	main axial flow velocity
V	number of stator vanes
v	circumferential velocity
x	axial coordinate

Greek

β	$\sqrt{1-M_x^2}$
$\Phi_{m\mu}$	radial eigenfunction [Eq.10]
ϕ	angular coordinate
$\Lambda_{m\mu}$	modal axial wave number [Eq.9]
θ	wake phase angle
ρ_0	ambient mass density
Ω	circumferential tip Mach number
ω	nondimensional frequency

Subscripts

0	source point, ambient
p	pressure
v	velocity
x	axial

This page is intentionally left blank.

Category 4 ---Fan Stator with Harmonic Excitation by Rotor Wake

NUMERICAL RESULTS OF LIFTING SURFACE THEORY

Masanobu Namba
Kumamoto Institute of Technology
Kumamoto, Japan

and

Johan B.H.M. Schulten
National Aerospace Laboratory NLR
Emmeloord, The Netherlands

1 Introduction

The Category 4 problem of the 3rd CAA Workshop addresses the noise resulting from rotor wakes impinging on a stator. Traditionally, the solution of the rotor-stator interaction noise problem is obtained by the application of a lifting surface method. These methods are based on the flow equations linearized about a uniform mean flow and have become a well-established technique. A strong point of lifting surface methods is the absence of numerical dissipation and dispersion errors, which so often prevent the application of regular CFD methods for noise problems. Therefore lifting surface results are very suitable as a benchmark test for CAA methods.

This paper gives the outline of the analytical methods based on the linearized lifting surface theory applied to Category 4, and gives the resulting numerical data. Unfortunately no CAA results for this problem were officially submitted at the 3rd workshop. It will be shown that this problem is worth to be retained as a test case for future CAA work.

2 Outline of Lifting Surface Theory

The original lifting surface theories by Namba (refs. 1, 2) and Schulten (refs. 3, 4) are formulated for a rotating annular cascade of straight or swept blades. Just to avoid unnecessary complexity we describe here the formulation applied to the present problem, i.e., a stator cascade of straight flat plates at zero stagger angle interacting with oncoming

sinusoidal gust. We also use the same notations as those used in the problem description by Hanson (App. C).

Interaction of the stator vanes with an oncoming sinusoidal gust with a circumferential velocity

$$v(r,\phi,x,t) = UV_1 e^{iB[\Omega x/U+\phi-\theta(r)-\Omega t]} \tag{1}$$

produces an unsteady blade loading. The pressure difference across the ν–th blade surface can be expressed as

$$\rho_0 U^2 \Delta C_p(r,x)\, e^{-i\omega t+i2\pi\nu B/V} : \nu = 0,1,...,V-1. \tag{2}$$

Here ρ_0 is the ambient air density and $\omega = B\Omega$. Then the wave equation for the acoustic pressure generated from the blades is given by

$$\left\{\nabla^2 - \frac{1}{a_0^2}\left(\frac{\partial}{\partial t} + U\frac{\partial}{\partial x}\right)^2\right\} p(r,\phi,x,t) = -\rho_o U^2 \frac{1}{r}\frac{\partial}{\partial\phi}\sum_{\nu=0}^{V-1}\int_h^R \frac{1}{r}\delta(r-r_0)\,dr_0$$
$$\times\int_0^b \Delta C_p(r_0,x_0)\, e^{-i\omega t+i2\pi\nu B/V}\delta(x-x_0)\,dx_0\,\delta(\phi-2\pi\nu/V). \tag{3}$$

The boundary condition at the duct walls is

$$\partial p/\partial r = 0 \quad \text{at} \quad r = R \quad \text{and} \quad r = h. \tag{4}$$

The formal solution can be expressed as

$$p(r,\phi,x,t) = \rho_0 U^2 \frac{1}{R^2} e^{-i\omega t}\int_h^R dr_0 \int_0^b \Delta C_p(r_0,x_0)\, K_p(r,\phi,x-x_0\,|\,r_0)\,dx_0. \tag{5}$$

Here the kernel function is obtained as the solution of the following equations:

$$\left\{\nabla^2 - \frac{1}{a_0^2}\left(-i\omega + U\frac{\partial}{\partial x}\right)^2\right\} K_p(r,\phi,x-x_0\,|\,r_0)$$
$$= -\frac{R^2}{r^2}\delta(r-r_0)\,\delta(x-x_0)\sum_{\nu=0}^{V-1} e^{i2\pi\nu B/V}\delta'(\phi-2\pi\nu/V), \tag{6}$$

$$\partial K_p/\partial r = 0 \quad \text{at} \quad r = R \quad \text{and} \quad r = h. \tag{7}$$

The solution is expressed as follows:

$$K_p(r,\phi,x|r_0) = \frac{V}{4\pi\beta^2}\sum_{k=-\infty}^{\infty}\sum_{\mu=0}^{\infty}\frac{im}{\Lambda_{m\mu}}\Phi_{m\mu}(r)\,\Phi_{m\mu}(r_0)$$
$$\times\exp\left[im\phi - i(M_x^2/\beta^2)\omega x/U - \Lambda_{m\mu}\,|\,x\,|/R\right] \tag{8}$$

Here

$$m = B - kV,\ M_x = U/a_0,\ \beta^2 = 1 - M_x^2.$$

Further $\Lambda_{m\mu}$ is defined by

$$\Lambda_{m\mu} = \begin{Bmatrix} \sqrt{A} & : & A \ge 0 \\ -i\,\mathrm{sgn}(\omega)\sqrt{-A} & : & A \le 0 \end{Bmatrix}, \quad A = \left\{k_{m\mu}^2 - (\omega R/U)^2 M_x^2/\beta^2\right\}/\beta^2. \tag{9}$$

Here $k_{m\mu}$ and $\Phi_{m\mu}(r):(\mu=0,1,2,...)$ are radial eigenvalues and eigenfunctions respectively of the following Sturm-Liouville boundary value problem.

$$\frac{R^2}{r}\frac{d}{dr}\left(r\frac{d\Phi_{m\mu}(r)}{dr}\right)+\left(k_{m\mu}^2-\frac{m^2R^2}{r^2}\right)\Phi_{m\mu}(r)=0, \tag{10}$$

$$d\Phi_{m\mu}(r)/dr=0 \quad \text{at} \quad r=R \quad \text{and} \quad r=h. \tag{11}$$

The eigenfunctions are normalized as follows:

$$\frac{1}{R^2}\int_h^R r\,\Phi_{m\mu}(r)\Phi_{m\nu}(r)\,dr=\delta_{\mu\nu}. \tag{12}$$

Therefore the mode shape function $\Psi_{m\mu}(r)$ defined in the problem description is given by

$$\Psi_{m\mu}(r)=\Phi_{m\mu}(r)/\left|\Phi_{m\mu}(r)\right|_{\max}. \tag{13}$$

The blade loading function $\Delta C_p(r,x)$ can be determined from the flow tangency condition on blade surfaces, which can be expressed by

$$\frac{1}{R^2}\int_h^R dr_0\int_0^b \Delta C_p(r_0,x_0)\,K_v(r,0,x-x_0\mid r_0)\,dx_0=-V_1e^{i\omega x/U-iB\theta(r)}, \tag{14}$$

where $K_v(r,\phi,x\mid r_0)$ is the upwash velocity kernel function given by

$$K_v(r,\phi,x\mid r_0)=-e^{i\omega x/U}\int_{-\infty}^{x} e^{-i\omega x/U}\,\frac{1}{r}\frac{\partial}{\partial\phi}K_p(r,\phi,x\mid r_0)\,dx$$

$$=-\frac{V}{4\pi\beta^2}\frac{R}{r}\sum_{k=-\infty}^{\infty}\sum_{\mu=0}^{\infty}\frac{m^2}{\Lambda_{m\mu}\left(i\omega R/(\beta^2U)+\Lambda_{m\mu}\,\mathrm{sgn}(x)\right)}\Phi_{m\mu}(r)\Phi_{m\mu}(r_0)e^{im\phi-i\left(M_x^2/\beta^2\right)\omega x/U-\Lambda_{m\mu}|x|/R}$$

$$+H(x)e^{i\omega x/U}\,\frac{VR}{2\pi r}\sum_{k=-\infty}^{\infty}\sum_{\mu=0}^{\infty}\frac{m^2}{k_{m\mu}^2+(\omega R/U)^2}\Phi_{m\mu}(r)\Phi_{m\mu}(r_0)e^{im\phi}. \tag{15}$$

The integral equation (14) for $\Delta C_p(r,x)$ should be solved numerically. Various methods are available. The methods used for the present problem by Namba and by Schulten are described in Appendix A and B respectively.

Finally the modal pressure amplitude $A_{m\mu}(x)$ defined by

$$p(r,\phi,x,t)=p_0\sum_{k=-\infty}^{\infty}\sum_{\mu=0}^{\infty}A_{m\mu}(x)\Psi_{m\mu}(r)e^{i(m\phi-B\Omega t)}, \tag{16}$$

can be calculated from

$$A_{m\mu}(x)=\gamma M_x^2\frac{imV}{4\pi\beta^2\Lambda_{m\mu}}\left[\Phi_{m\mu}(r)\right]_{\max}$$

$$\times\frac{1}{R^2}\int_h^R dr_o\int_0^b \Delta C_p(r_0,x_0)\Phi_{m\mu}(r_0)\exp\left[-\frac{M_x^2}{\beta^2}\frac{\omega}{U}(x-x_0)-\frac{\Lambda_{m\mu}}{R}\mid x-x_0\mid\right]dx_0, \tag{17}$$

where $\gamma(=1.4)$ is the specific heat ratio of air.

3 Numerical Results

Numerical values of the modal pressure amplitude $A_{m\mu}(x)$ calculated by Namba and Schulten are given in Table 1 and Tables 2.1 – 2.10. To save space, circumferential wave numbers are confined to the smallest two; m=16 and m=-8. The other modal pressure amplitudes are extremely small. The agreement between Namba's and Schulten's data is fairly good. The discrepancies will come from various numerical processes in solving the integral equation (14) and computing integrals in equation (17). In particular the exceptional large discrepancy observed for M_T = 0.433 of the narrow annulus (Table 1) is due to the fact that the condition is very close to the resonance $(\Lambda_{m\mu} = 0)$ of the mode of m = -8, μ = 0.

Table 3 and Figure 1 show a comparison between the unsteady lift coefficient C_L $(= \int_0^b \Delta C_p(r,x)dx/(bV_1))$ at mid-span of the narrow annulus cascade and that of the corresponding 2-dimensional cascade. It is clear that the flow field of the narrow annulus cascade is nearly two-dimensional. On the other hand the validity of the 2D code used to compute the two-dimensional problems was ascertained from the fact that it exactly reproduces Figure 5(a) of Hall and Verdon (ref.5), which was computed with Smith's code.

It should be noted that in the full annulus cases, all modes are cut-off for M_T=0.470, only one mode (m=-8, μ=0) is cut-on for M_T =0.522 and M_T =0.574, and two modes (m=-8, μ =0), (m=-8, μ =1) are cut-on for M_T =0.783. Certainly the amplitudes of cut-off modes are smaller than those of cut-on modes, but they are not extremely small. This is because the axial positions one chord away from the leading and trailing edges are not far enough for the cut-off modes to decay out. Therefore at more distant positions the difference in the magnitude between cut-on and cut-off modes will be more pronounced. However, to compute pressures at such distant positions by CAA methods may worsen the problem of numerical dissipation and dispersion.

In Figure 2 a comparison is made between the results of Namba and Schulten. The pressure jump distribution (ΔC_p based on $\rho_0 U^2$ /2) at mid-span for the full annulus is compared for the highest tip speed of the rotor investigated in the present study (M_T = 0.783). It is clear that the agreement between both methods is very good. Only in the aft portion of the chord some small discrepancies are visible.

A three-dimensional view on the pressure jump distribution over the whole reference vane is given in Figure 3. In this case the incident velocity field is in phase along the span (q = 0.0, see App. C) which is clearly reflected by the behavior of the pressure jump in the vicinity of the leading edge. In the aft portion of the vane some mild spanwise variation is discernible which results from the three-dimensionality of the stator.

As shown in Figure 4 the response of the stator is quite sensitive to the spanwise phasing of the impinging field which is characterized by q = 1.5 in this case. This spanwise

periodicity is only recognized in the pressure jump distribution in the immediate vicinity of the leading edge. Further downstream, the spanwise response is closer to one full wavelength. But the most remarkable observation is the very large amplitude of the response, which points to some kind of near-resonance behavior. This may have to do with the (intentional, see problem description) similarity of the excitation with the acoustic radial mode shapes for $\mu = 1$ (cut-on) and $\mu = 2$ (cut-off) ($m = -8$).

The contrast with the results for $q = 3.0$, presented in Figure 4, is striking. It is hardly imaginable that the only difference in the incident field is a spanwise phasing twice as high as in Figure 3. This phasing can still be observed in the leading edge portion of the vane but vanishes downstream. It is reconfirmed even stronger that the spanwise phasing is crucial to the stator response.

The $q = 3.0$ case was taken for another comparison between Namba's and Schulten's results. In Figure 5 the pressure jump is compared along a spanwise line located at 6 percent of the chord. The agreement is quite satisfactory but some slight discrepancies near the hub and the casing can be observed. Figure 6 gives the results along a spanwise line at 20 percent of the chord. Here some more discrepancies are visible, not only at hub and casing but also in the mid-span region. However, it should not be overlooked that the scale is four times larger than in the previous figure. It seems as if the spanwise waviness first starts to disappear in the mid-span region. Note that the pressure jump should have a zero derivative at hub and casing due to the hard wall boundary conditions [Eq.(4)]. Relatively large discrepancies are observed along the 50 percent line in Figure 7. Only one full spanwise wavelength can be observed here. Finally, in Figure 8 the pressure jump along the 90 percent line shows a better, although not a perfect, agreement. In general, it seems that closer to the leading and trailing edges the agreement is better than in the inner portion of the vane. It is noted that seemingly small discrepancies in the pressure jump can affect the modal amplitudes more seriously. This may be the reason that, occasionally, the agreement in the modal amplitudes is not as good as was expected by the authors on beforehand.

4 Concluding remarks

The Category-4 benchmark problem was successfully computed by two lifting surface methods. The problem definition was well chosen to include some interesting near-resonance effects.

Comparison of the results of both methods showed good agreement on the whole. It appeared that relatively small discrepancies in the pressure jump distribution could lead to relevant discrepancies in the modal amplitudes. It would be helpful if in future CAA

benchmarking of the rotor stator interaction problem, attention will also be paid to the prediction of the pressure jump distribution rather than only to the modal amplitudes.

5 References

1. Namba, M., “Three-Dimensional Flows,” *AGARD Manual on Aeroelasticity in Axial Flow Turbomachines, Vol.1, Unsteady Turbomachinery Aerodynamics* (AGARD-AG-298). M.F. Platzer and F.O. Carta, eds., Neuilly sur Seine, France, Chap. 4, 1987.
2. Namba, M. and Ishikawa, A., “Three-Dimensional Aerodynamic Characteristics of Oscillating Supersonic and Transonic Annular Cascades”, *ASME Journal of Engineering for Power*, **105**, 1983, pp.138-146.
3. Schulten, J.B.H.M., “Sound Generated by Rotor Wakes Interacting with a Leaned Vane Stator”, *AIAA Journal*, **20**-**10**, 1982, pp.1352-1358, (also NLR MP 80041 U).
4. Schulten, J.B.H.M., "Vane sweep effects on rotor/stator interaction noise," *AIAA Journal*, Vol.35, No.6, June 1997, pp.945-951, (also NLR TP 96135 U).
5. Hall, K.C. and Verdon, J.M., “Gust Response Analysis for Cascades Operating in Nonuniform Mean Flows,” *AIAA Journal*, **29-8**, 1991, pp.1463-1471.
6. Abramowitz, M., Stegun, I.A., *Handbook of Mathematical Functions*, Dover Publications, New York, 1968.
7. Bender, C.M., Orszag, S.A., *Advanced Mathematical Methods for Scientists and Engineers*, McGraw-Hill, 1978.

Appendix A Namba's Method

The kernel function of the integral equation (14) contains singularities of $1/(x-x_0)$ and $\log|x-x_0|$. It is desirable to calculate the principal values analytically rather than numerically. To do so it is necessary to extract the singular parts from the kernel function. But it is not easy because the eigenfunctions $\Phi_{m\mu}(r)$ do not approach to definite values as *m* goes to infinity.

To cope with this difficulty Namba (refs. 1,2) developed the method of finite radial mode expansion. The essence of the method is to approximate the eigenfunction by a finite series expansion of the form:

$$\Phi_{m\mu}(r)=\sum_{\ell=0}^{L-1} B_{\mu\ell}^{(m)}\Phi_{0\ell}(r)\,. \tag{A1}$$

Then the coefficients $B_{\mu\ell}^{(m)}$ can be determined as eigenvectors of a real symmetric matrix, and we can calculate the limit values of $\lim_{m\to\infty} B_{\mu\ell}^{(m)} = B_{\mu\ell}^{(\infty)}$. Therefore the approximate eigenfunctions have definite limit functions of $\Phi_{\infty\mu}(r)$. Expressing the kernel function in terms of $\Phi_{0\mu}(r)$ or $\Phi_{\infty\mu}(r)$, we can easily extract the singular parts of the kernel function.

The unknown blade loading function is expressed in terms of double mode function series:

$$\Delta C_p(r,x)=\sum_{\ell=0}^{L-1}\Phi_{\infty\ell}(r)\left\{A_{\ell 0}\cot\frac{\xi}{2}+\sum_{j=1}^{J-1}A_{\ell j}\sin(j\xi)\right\},\quad x=(1-\cos\xi)b/2, \tag{A2}$$

and the principal values can be analytically calculated. The problem reduces to algebraic equations for the coefficients $A_{\ell j}$. This formulation also enables us to calculate the integrals in equation (17) analytically. The accuracy of the numerical solution essentially depends on the numbers of retained terms *L* and *J*. To solve the present problem *L*=21 and *J*=11 are adopted. It takes about 65 seconds to compute one case on PC of Celeron 350 MHz.

Appendix B Schulten's Method

The first step to the numerical solution of Eq.14 is the representation of the unknown ΔC_p. The chordwise expansion is identical to Namba's given in Eq. (A2). However, for the spanwise direction a Chebyshev (1st kind) series is adopted. This series can be considered as a Fourier cosine series in the variable ψ where

$$\cos\psi = 2(r-h)/(R-h) - 1 \qquad \text{(B1)}$$

To solve the integral equation (14) numerically, a Galerkin procedure is followed. This means that both sides of the equation are projected on a set of orthogonal basis functions. The advantage of a Galerkin method over a collocation method is that the number of points on the vane surface can be taken (much) larger than the number of unknowns . The Galerkin method yields the least squares fit to the point values on the vane. The Galerkin basis functions used are Chebyshev 1st kind for the spanwise direction and 2nd kind for the chordwise direction. Gauss-Lobatto integration formulae (ref. 6) are used to evaluate the integrals.

The number of required projections is taken to be sufficient to capture the right hand side to a pre-set accuracy. In the present study an accuracy of 0.004 relative to the largest right hand side term was adopted throughout. Further, the expansions are taken sufficiently large to resolve the shortest acoustic wavelengths upstream and downstream as well as in spanwise direction. The final criterion is that also the hydrodynamic wave is accurately resolved. For the most demanding case (M_T = 0.783, q = 3.0), the maximum number of required projections was 17 spanwise × 9 chordwise. These numbers were also taken for J and L respectively in the expansion of ΔC_p.

After taking the Galerkin projections the integral equation turns into a matrix equation the left hand side of which contains a series in k which essentially is a Fourier series in the circumferential co-ordinate. This is a slowly convergent series with terms behaving as $1/k^2$ asymptotically. To obtain an accuracy of, say, ε = 0.004 with respect to the largest element in its row of the matrix would require something in the order of $1/\varepsilon$ = 250 terms. This would be very hard computationally. Therefore a 2nd order Richardson extrapolation (ref.7) is applied to the k-series. For the most demanding case (see above) this limits k_{max} to 18. Nevertheless, the total computing time for this matrix is about 40 hours on a 300 MHz PC.

In the present method the evaluation of the infinite radial series over μ as occurring in Eqs. (8) and (15) is handled quite differently from Namba's method. As described in ref.4, the series can be replaced by an integral in the complex α-plane, where α is the wave number in x-direction. By deforming the contour of integration away from the poles, a smooth integrand is obtained that can be accurately integrated numerically. The only difficulty is encountered for a case very close to duct mode resonance (cut-on) when the path of integration has to pass two poles very closely. This integral representation is

especially advantageous for vanes of arbitrary shape. For the unswept vanes with constant chord of the present configuration the integral representation is considerably more time consuming than Namba's method.

Appendix C Benchmark Problem Description

Benchmark Problems

Category 4 --- Fan Stator with Harmonic Excitation by Rotor Wake [1]

Introduction

These problems are simple representations of rotor wake/stator interaction in axial flow fans. They include much of the blade row scattering/spinning mode propagation physics of the real problem but are still in the realm of Green's function/panel methods, so that results can be checked. They are problems that anyone developing a CFD/CAA code for fans might do for code checkout and should be doable with several codes in existence today. The vane/blade ratio of 3/2 will make the problems easier for codes based on periodic boundary conditions.

The first cases are for excitation that is nearly 2D (constant along the span). Then, the problem is made progressively more 3-dimensional by varying the phase of the excitation along the span. This simulates the situation (typical of turbofans) where more than one wake from the rotor intersects a vane at the same time. A high hub/tip ratio case has been added for a check against 2D (S.N. Smith) theory.

3D results will be checked by comparison with one or more well-known panel methods. In particular, Professor M. Namba from Kyushu University in Japan and Dr. J.B.H.M. Schulten from the National Aerospace Laboratory NLR in the Netherlands will be asked to provide results from their lifting surface codes.

[1] Prepared by Donald B. Hanson, Pratt & Whitney,

Mean Flow and Geometry

Assume standard day conditions for speed of sound a_0 and pressure p_0 and uniform axial flow at M_x=0.5. The duct is infinite in both directions with constant outer radius R (which need not enter the calculations) and hub/tip ratio h/R. The stator consists of constant chord, zero thickness vanes with cords parallel to the fan axis. (If zero thickness causes problems, use 10th standard cascade airfoils with camber removed. Ordinates will be supplied by D. Hanson on request.) Gap/chord =1.0 at the tip. Blade/vane counts are B=16 and V=24. The duct and the 24 vanes are the only surfaces.

Wake Representation

In the x,r,ϕ co-ordinate system, excitation for the problem is a convected wave of radial vorticity representing a harmonic rotor wake. It produces a velocity perturbation in the ϕ direction given by (the real part of)

$$v(r,\phi,x,t) = U\sum_{n=0}^{\infty} V_n e^{inB[\Omega x/U+\phi-\theta(r)-\Omega t]} \tag{1}$$

U is the axial flow speed $a_0 M_x$ and Ω is the rotor (and wake) angular velocity. Consider only the blade passing frequency (BPF) fundamental, n=1, with upwash amplitude equal to 0.1 radian, V_n=0.1. Reduced frequency $\omega b/U = nB\,\Omega b/U$ is constant over the span. The function giving the radial dependence is

$$\theta(r) = -(2\pi q/B)[(r-h)/(R-h)] \tag{2}$$

$\theta(r)=-2\pi q/B$ is the phase shift along the stator span. For q=0, the excitation is in phase from root to tip of the stator. When q=2, there are 2 wakes intersecting each stator vane, on average. The minus sign leading (2) causes the wake at the stator root to lead that at the tip as in typical fan designs. In the convention of (1), the inter-vane phase angle is $2\pi nB/V$ (counting vanes in the direction of rotor rotation).

Cases for Computation

Some participants may want to test their codes in a narrow annulus mode first for comparison with the Smith code before moving on to the 3D cases. Results from the Smith code will be supplied to participants on request. The appendix provides background from standard fan noise theory (Tyler-Sofrin) that was used to determine the 3D cases.

Narrow Annulus

To approximate 2D, run hub/tip ratio h/R=0.98 and no radial variation, $\theta(r)$=0. In this case the cut-off ratio of the response waves is given by

$$\xi = (nB/m)\,(M_T/\beta) \tag{3}$$

where $m=nB-kV$ is their spinning mode order and $\beta^2=1-M_x^2$. Run a BPF (n=1) series around cut-on plus two cases well above cut-on as follows

ξ	M_T	**Comments**
0.9	0.3897	cut off (sub-resonant)
1.0	0.4330	Resonant
1.1	0.4763	m=-8 is cut on
1.5	0.6495	m=-8 is cut on

The chord-based reduced gust frequency $\omega b/U = nB\Omega\ b/(a_0 M) = nB\Omega R/(a_0 M) b/R = (2\pi nB/V)(M_T/M)$ where V=24 is the vane count. The duct radius-based acoustic reduced frequency $\omega R/a_0 = nBM_T$.

To present results, give the complex coefficients A_m, which are defined by the expression for the pressure perturbation

$$p(x,r,\phi,t) = p_0 \sum_{k=-\infty}^{\infty} A_m(x) e^{i(m\phi - nB\Omega t)} \tag{4}$$

Do this for axial locations one chord upstream and one chord downstream of the stator (x=-b and +2b) and present results by filling in the following table with complex values of A_m.

M_T	**Upstream Waves, x=-b**				**Downstream Waves, x=+b**			
	m=40	m=16	m=-8	m=-32	m=40	m=16	M=-8	m=-32
0.3897								
0.4330								
0.4763								
0.6495								

Full Annulus

These are all for h/R=0.5. The first series is for zero radial phase variation and has the same cut-off ratios as the narrow annulus case above. They pass through cut-on via increases in rotor speed.

q	ξ	M_T
0	0.9	0.470
0	1.0	0.522
0	1.1	0.574
0	1.5	0.783

The second series starts with the ξ=1.5 case above and progresses through cut-off by increasing the phase variation of the excitation along the radius. This represents the sweep of a rotor wake.

q	ξ@μ=q	M_T
0	**1.50**	**0.783**
0.5		0.783
1.0	1.05	0.783
1.5		0.783
2.0	**0.83**	**0.783**
2.5		0.783
3.0	0.65	0.783

The middle column is the cut-off ratio of the acoustic mode with the same number of radial zero crossings as the excitation wave.

Present results as the complex coefficients $A_{nm\mu}$, which are defined by the pressure field modal expansion

$$p_n(r,\phi,x,t) = p_0 \sum_{k=-\infty}^{\infty} \sum_{\mu=0}^{\infty} A_{nm\mu}(x)\Psi_{m\mu}(r)e^{i(m\phi - nB\Omega t)} \tag{5}$$

where $\Psi_{m\mu}(r)$ is the radial mode shape (discussed below) and, again, $m=nB-kV$. Do this for axial locations one chord upstream and one chord downstream of the stator ($x=-b$ and $+2b$). Present results in modal form by filling in tables like the following for each condition run.

Radial mode order μ	**Upstream Waves, *x*=-*b***				**Downstream Waves, *x*=+*b***			
	m=40	m=16	m=-8	m=-32	m=40	m=16	m=-8	m=-32
0								
1								
2								
3								
4								

For participants wishing to minimize the number of cases to run, the highest priority should be the q=0 and q=2 cases at M_T=0.783 shown above in bold type.

The mode amplitudes will depend on the convention used for the radial mode shapes $\Psi_{m\mu}(r)$. These are the duct eigenmodes described by Tyler and Sofrin. However, for easy comparison with 2D results, a different normalization is used. The extreme value of each mode is set to +1. On request, a FORTRAN routine will be sent to participants that allows Fourier analysis of the pressure perturbation in a constant x-plane to determine the complex mode amplitudes $A_{nm\mu}$.

References

1.Smith, S.N., "Discrete Frequency Sound Generation in Axial Flow Turbomachines", Aeronautical Research Council Reports and Memoranda, R. & M. No. 3709, HMSO, London, 1973.

2.Tyler, J.M. & Sofrin, T.G., ``Axial Flow Compressor Noise Studies", *SAE Trans.*, Vol. 70, 1962, 308--332.

Appendix --- Background from Spinning Mode Theory

In the traditional treatment of acoustic waves in annular ducts with uniform axial flow, the pressure disturbance at the n_{th} harmonic of blade passing frequency can be expressed in the following modal form

$$p_n(r,\phi,x,t) = p_0 \sum_{k=-\infty}^{\infty}\sum_{\mu=0}^{\infty} A_{nm\mu}\Psi_{m\mu}(r)e^{i(\gamma_{nm\mu}x+m\phi-nB\Omega t)} \tag{6}$$

where the circumferential order of the spinning mode order

$$m = nB - kV \tag{7}$$

Ω is the angular speed of the rotor and $\Psi_{m\mu}(r)$ are the radial mode functions, which are combinations of Bessel functions. From the form of the exponential in (6), it can be deduced that the spin Mach number of the mode at the outer wall is

$$M_S = (nB/m)\, M_T \tag{8}$$

where $M_T=(\Omega R/a_0)$ is the rotor tip rotational Mach number. Since cut-on is determined by the mode spin speed, we must identify the most cut on mode. The following table, for n=1 (BPF)

k	m	nB/m
-1	40	0.40
0	16	1.00
1	-8	-2.00
2	-32	-0.50

shows that the fastest mode is the fundamental interaction mode m=B-V. This is an 8 lobe pattern rotating in the direction opposite the rotor at twice the rotor speed.

The cut-off ratio is the ratio of the rpm to the cut-on rpm. This is given by

$$\xi = (nB/m)\,[M_T/(\beta\, M^*_m)] \tag{9}$$

which is also the ratio of the mode spin speed to the spin speed $\beta\, M^*_m$ at which the mode cuts on. $M^*_m = k'^{\sigma}_{m\mu}/m$ can be computed by looking up $k'^{\sigma}_{m\mu}$ in the Tyler-Sofrin paper. The correction for axial Mach number is $\beta^2=1-M^2_x$. Note that $M^*_m=1.0$ for 2D cases. The required information for our situation at BPF with an m=-8 mode in a duct with 0.5 hub/tip ratio and 0.5 axial Mach number is

μ	M^*_m	βM^*_m	M^*_T
0	1.205	1.043	0.522
1	1.725	1.494	0.747
2	2.168	1.877	0.939
3	2.767	2.396	1.198

where M^*_T is the rotor tip Mach number for cuton of the -8,μ mode.

Tables

Table 1. Narrow Annulus q =0

Upstream Waves: x=-b								
	m=16				m =-8			
M_T	Real		Imag		Real		Imag	
	Namba	Schulten	Namba	Schulten	Namba	Schulten	Namba	Schulten
0.3897	-2.422E-05	-1.930E-05	9.174E-06	8.120E-06	-5.067E-03	-5.407E-03	1.924E-03	2.231E-03
0.4330	-9.952E-05	-8.599E-05	-1.874E-05	-5.001E-06	-1.142E-03	2.083E-03	-2.170E-04	3.459E-04
0.4763	-1.043E-04	-1.033E-04	-7.110E-05	-6.823E-05	-7.603E-03	-7.538E-03	1.837E-03	2.055E-03
0.6495	-8.334E-05	-1.074E-04	-4.261E-04	-4.033E-04	7.577E-03	7.364E-03	-1.814E-03	-2.453E-03
Downstream Waves: x=+2b								
	m =16				m =-8			
M_T	Real		Imag		Real		Imag	
	Namba	Schulten	Namba	Schulten	Namba	Schulten	Namba	Schulten
0.3897	-6.945E-05	-7.063E-05	3.666E-05	3.999E-05	8.584E-03	8.734E-03	-4.532E-03	-4.943E-03
0.4330	-5.302E-05	-4.718E-05	1.641E-05	8.436E-06	1.715E-02	3.410E-03	-5.298E-03	-6.981E-04
0.4763	-3.587E-05	-3.619E-05	1.999E-05	2.090E-05	1.050E-02	1.061E-02	1.604E-02	1.556E-02
0.6495	2.529E-05	1.903E-05	1.282E-05	5.809E-06	-1.120E-02	-9.946E-03	5.684E-03	5.870E-03

Table 2.1 Full Annulus : q=0, M_T =0.470

Upstream Waves, x=-b								
	m =16				m =-8			
	Real		Imag		Real		Imag	
	Namba	Schulten	Namba	Schulten	Namba	Schulten	Namba	Schulten
μ = 0	-6.635E-05	-5.482E-05	1.687E-05	1.047E-05	-2.073E-03	-2.881E-03	-1.955E-03	-1.456E-03
μ = 1	-7.690E-06	-8.411E-06	-5.077E-06	-3.579E-06	1.894E-04	2.546E-04	4.300E-04	2.595E-04
μ = 2	-1.500E-06	-1.950E-06	-1.921E-06	-1.272E-06	2.341E-05	3.635E-05	6.261E-05	4.026E-05
μ = 3	-3.851E-07	-5.237E-07	-5.331E-07	-4.021E-07	1.312E-06	1.958E-06	2.356E-06	2.221E-06
μ = 4	-4.975E-08	-7.115E-08	-7.526E-08	-6.257E-08	5.220E-08	8.742E-08	1.119E-07	1.097E-07

Downstream Waves, x=+2b								
	m =16				m =-8			
	Real		Imag		Real		Imag	
	Namba	Schulten	Namba	Schulten	Namba	Schulten	Namba	Schulten
μ = 0	-7.287E-05	-6.680E-05	3.060E-05	3.998E-05	9.484E-03	9.296E-03	-4.826E-03	-5.798E-03
μ = 1	-2.814E-06	-3.457E-06	3.402E-06	3.081E-06	-3.249E-06	9.737E-05	-2.600E-04	-1.776E-04
μ = 2	-7.340E-08	-3.810E-07	6.725E-07	4.967E-07	-1.264E-05	-1.055E-07	-2.353E-05	-1.290E-05
μ = 3	3.477E-09	-5.530E-08	1.562E-07	1.054E-07	-1.534E-07	-1.315E-07	-8.371E-07	-4.555E-07
μ = 4	3.018E-09	-2.657E-09	1.857E-08	1.123E-08	-1.415E-08	-1.294E-08	-2.883E-08	-1.219E-08

Table 2.2 Full Annulus : q =0, M_T =0.522

Upstream Waves, x=-b								
	m =16				m =-8			
	Real		Imag		Real		Imag	
	Namba	Schulten	Namba	Schulten	Namba	Schulten	Namba	Schulten
μ = 0	-1.224E-04	-1.190E-04	-8.522E-05	-5.906E-05	1.792E-02	1.529E-02	1.153E-02	5.181E-03
μ = 1	-3.614E-06	-6.159E-06	-7.968E-06	-1.302E-05	-4.648E-04	-1.110E-05	4.768E-04	1.032E-03
μ = 2	1.995E-07	-5.846E-07	-1.308E-06	-3.141E-06	-5.493E-05	-1.412E-05	3.837E-05	1.073E-04
μ = 3	5.952E-08	-4.987E-08	-2.994E-07	-8.420E-07	-1.006E-06	-9.035E-07	1.465E-06	4.692E-06
μ = 4	9.765E-09	5.772E-09	-3.386E-08	-1.138E-07	-4.796E-08	-5.519E-08	4.262E-08	1.867E-07
Downstream Waves, x=+2b								
	m =16				m =-8			
	Real		Imag		Real		Imag	
	Namba	Schulten	Namba	Schulten	Namba	Schulten	Namba	Schulten
μ = 0	-6.237E-05	-7.757E-05	1.613E-06	2.344E-05	3.928E-02	4.724E-02	-5.248E-03	-9.905E-03
μ = 1	-2.969E-06	-7.565E-07	6.235E-06	4.294E-06	6.465E-05	-3.512E-04	-8.589E-04	-4.707E-04
μ = 2	-2.241E-07	4.121E-07	1.726E-06	9.459E-07	-3.234E-06	-4.480E-05	-8.308E-05	-4.237E-05
μ = 3	-3.758E-08	1.651E-07	4.150E-07	2.376E-07	1.173E-07	-1.916E-06	-2.440E-06	-1.623E-06
μ = 4	-2.497E-09	2.756E-08	5.147E-08	3.011E-08	-3.218E-09	-8.002E-08	-9.167E-08	-5.717E-08

Table 2.3 Full Annulus, q =0, M_T =0.574

Upstream Waves, x=-b								
	m =16				m =-8			
	Real		Imag		Real		Imag	
	Namba	Schulten	Namba	Schulten	Namba	Schulten	Namba	Schulten
μ = 0	-8.222E-05	-9.639E-05	-1.274E-04	-1.175E-04	-1.970E-02	-1.725E-02	7.111E-05	4.671E-03
μ = 1	-7.084E-06	-5.057E-06	-8.093E-06	-6.979E-06	-1.293E-05	-4.105E-04	1.297E-04	1.377E-04
μ = 2	-1.488E-06	-8.443E-07	-1.246E-06	-9.783E-07	1.088E-05	-2.539E-05	9.418E-06	4.041E-06
μ = 3	-4.026E-07	-2.110E-07	-3.127E-07	-1.884E-07	1.214E-06	-4.166E-07	1.065E-06	7.052E-08
μ = 4	-5.554E-08	-2.855E-08	-3.953E-08	-1.787E-08	5.876E-08	7.636E-10	3.681E-08	-5.059E-09
Downstream Waves, x=+2b								
	m =16				m =-8			
	Real		Imag		Real		Imag	
	Namba	Schulten	Namba	Schulten	Namba	Schulten	Namba	Schulten
μ = 0	-4.189E-05	-4.431E-05	1.166E-05	1.088E-05	6.598E-03	5.028E-03	2.515E-02	2.561E-02
μ = 1	-4.419E-06	-3.181E-06	5.204E-06	6.692E-06	4.831E-04	2.696E-04	-8.430E-04	-1.146E-03
μ = 2	-8.140E-07	-4.852E-07	1.313E-06	1.633E-06	3.338E-05	1.562E-05	-6.704E-05	-9.173E-05
μ = 3	-1.816E-07	-9.871E-08	3.064E-07	4.253E-07	1.042E-06	4.736E-07	-1.848E-06	-3.356E-06
μ = 4	-2.087E-08	-1.003E-08	3.725E-08	5.548E-08	3.322E-08	1.101E-08	-6.705E-08	-1.176E-07

Table 2.4 Full Annulus q =0, M_T =0.783

Upstream Waves, x=-b								
	m =16				m =-8			
	Real		Imag		Real		Imag	
	Namba	Schulten	Namba	Schulten	Namba	Schulten	Namba	Schulten
$\mu = 0$	2.541E-04	1.486E-04	-6.945E-04	-6.906E-04	3.493E-03	5.140E-03	1.125E-02	1.056E-02
$\mu = 1$	6.726E-06	6.191E-06	-2.322E-05	-2.409E-05	-6.674E-03	-7.631E-03	-1.811E-02	-1.747E-02
$\mu = 2$	1.188E-06	8.004E-07	-3.107E-06	-3.231E-06	-1.816E-04	-8.145E-05	1.243E-04	1.072E-04
$\mu = 3$	2.634E-07	1.324E-07	-7.104E-07	-7.178E-07	-3.028E-06	-1.370E-06	4.329E-06	4.021E-06
$\mu = 4$	2.739E-08	1.044E-08	-8.201E-08	-8.572E-08	-6.474E-08	-2.451E-08	1.053E-07	1.271E-07

Downstream Waves, x=+2b								
	m =16				m =-8			
	Real		Imag		Real		Imag	
	Namba	Schulten	Namba	Schulten	Namba	Schulten	Namba	Schulten
$\mu = 0$	2.088E-05	-3.081E-05	-1.024E-04	-1.007E-04	-1.707E-02	-1.497E-02	-1.594E-03	-2.731E-04
$\mu = 1$	-1.025E-05	-8.833E-06	5.674E-06	5.207E-06	7.702E-03	8.603E-03	1.731E-02	1.564E-02
$\mu = 2$	-1.824E-06	-1.898E-06	1.295E-06	1.428E-06	1.022E-04	1.729E-04	-1.558E-04	-2.034E-04
$\mu = 3$	-3.404E-07	-4.196E-07	2.745E-07	3.240E-07	1.589E-06	3.048E-06	-2.310E-06	-3.024E-06
$\mu = 4$	-3.730E-08	-4.788E-08	3.130E-08	3.878E-08	6.709E-08	8.474E-08	-6.732E-08	-8.943E-08

Table 2.5 Full Annulus q =0.5, M_T =0.783

Upstream Waves, x=-b								
	m =16				m =-8			
	Real		Imag		Real		Imag	
	Namba	Schulten	Namba	Schulten	Namba	Schulten	Namba	Schulten
μ = 0	2.295E-04	2.607E-04	5.566E-04	5.036E-04	-7.152E-03	-7.285E-03	1.333E-05	2.304E-05
μ = 1	1.703E-05	2.046E-05	5.059E-06	1.080E-05	1.109E-02	1.241E-02	-1.667E-02	-1.951E-02
μ = 2	3.463E-06	3.173E-06	-2.646E-06	-3.587E-06	-5.908E-04	-2.929E-04	5.684E-04	9.876E-04
μ = 3	8.275E-07	6.741E-07	-8.096E-07	-1.316E-06	-8.793E-06	-5.157E-06	8.222E-06	1.661E-05
μ = 4	5.814E-08	6.093E-08	-9.399E-08	-1.778E-07	3.554E-08	-4.438E-08	1.225E-07	3.835E-07
Downstream Waves, x=+2b								
	m =16				m =-8			
	Real		Imag		Real		Imag	
	Namba	Schulten	Namba	Schulten	Namba	Schulten	Namba	Schulten
μ = 0	-1.625E-05	-1.893E-05	-3.463E-05	-2.728E-05	1.132E-02	8.825E-03	-1.370E-02	-1.405E-02
μ = 1	-1.517E-05	-7.840E-06	8.852E-06	1.166E-05	5.529E-03	8.351E-03	2.134E-02	1.706E-02
μ = 2	-1.591E-06	-2.141E-06	-5.765E-07	-8.008E-07	-1.701E-04	2.677E-04	5.495E-04	7.376E-04
μ = 3	-1.457E-07	-5.001E2507	-4.244E-07	-5.714E-07	-2.808E-06	4.390E-06	9.158E-06	1.251E-05
μ = 4	-1.139E-08	-5.981E-08	-5.678E-08	-8.514E-08	-2.334E-09	1.255E-07	1.476E-07	2.690E-07

Table 2.6 Full Annulus q =1.0 M_T =0.783

Upstream Waves x=-b								
	m =16				m =-8			
	Real		Imag		Real		Imag	
	Namba	Schulten	Namba	Schulten	Namba	Schulten	Namba	Schulten
$\mu = 0$	-2.151E-04	-2.711E-04	-2.391E-04	-3.082E-04	1.063E-03	3.948E-03	1.310E-03	1.371E-03
$\mu = 1$	-1.491E-05	-2.915E-05	3.802E-06	1.870E-05	8.336E-03	1.860E-02	1.009E-02	1.338E-02
$\mu = 2$	5.645E-06	7.245E-06	1.242E-06	-1.626E-09	-1.471E-03	-2.266E-03	-7.834E-04	3.048E-04
$\mu = 3$	7.557E-07	1.952E-06	5.352E-07	-1.631E-07	-4.147E-08	-1.947E-05	-1.607E-05	1.823E-07
$\mu = 4$	-6.994E-09	1.789E-07	8.519E-08	-1.049E-09	2.238E-07	-2.077E-07	-3.766E-07	-1.231E-07
Downstream Waves, x=+2b								
	m =16				m =-8			
	Real		Imag		Real		Imag	
	Namba	Schulten	Namba	Schulten	Namba	Schulten	Namba	Schulten
$\mu = 0$	1.419E-04	3.216E-05	-1.141E-04	-1.743E-04	1.987E-03	4.907E-03	9.959E-03	8.607E-03
$\mu = 1$	-3.118E-05	-3.213E-05	-1.251E-05	7.415E-06	-1.679E-02	-5.257E-03	2.178E-02	2.413E-02
$\mu = 2$	1.238E-06	1.370E-06	-4.899E-07	-2.064E-06	-1.635E-03	-1.746E-03	-4.069E-04	8.727E-04
$\mu = 3$	1.155E-06	1.267E-06	1.501E-07	-8.691E-07	-2.597E-05	-2.838E-05	-6.972E-06	1.425E-05
$\mu = 4$	1.567E-07	1.764E-07	2.462E-08	-1.140E-07	-4.218E-07	-4.800E-07	-9.487E-08	2.750E-07

Table 2.7 Full Annulus q =1.5, M_T =0.783

Upstream Waves, x=-b								
	m =16				m =-8			
	Real		Imag		Real		Imag	
	Namba	Schulten	Namba	Schulten	Namba	Schulten	Namba	Schulten
$\mu = 0$	2.151E-04	3.234E-04	1.990E-04	1.278E-04	-3.762E-03	-4.124E-03	-2.203E-04	2.379E-03
$\mu = 1$	1.652E-06	-1.293E-05	-1.816E-05	-2.847E-05	-8.479E-03	-1.073E-02	-3.723E-03	5.808E-03
$\mu = 2$	1.008E-06	2.192E-06	5.194E-06	6.159E-06	3.715E-04	-6.205E-04	-1.112E-03	-1.650E-03
$\mu = 3$	7.308E-08	7.286E-07	-5.011E-07	4.380E-07	1.778E-05	2.586E-06	2.463E-05	8.658E-06
$\mu = 4$	-2.661E-07	-1.646E-07	-1.873E-07	-3.530E-08	1.840E-06	1.473E-06	2.679E-07	-7.326E-08

Downstream Waves, x=+2b								
	m =16				m =-8			
	Real		Imag		Real		Imag	
	Namba	Schulten	Namba	Schulten	Namba	Schulten	Namba	Schulten
$\mu = 0$	7.441E-05	1.402E-04	1.266E-04	2.861E-05	-1.104E-03	-1.276E-03	-4.053E-03	-1.952E-03
$\mu = 1$	1.771E-06	-1.460E-05	-2.379E-05	-2.232E-05	-1.290E-02	-1.342E-02	-1.786E-03	7.195E-03
$\mu = 2$	-4.071E-07	9.430E-07	1.695E-06	1.643E-06	2.264E-04	-8.604E-04	-1.431E-03	-1.384E-03
$\mu = 3$	-1.939E-07	6.728E-07	1.080E-06	1.071E-06	4.634E-06	-1.351E-05	-2.161E-05	-2.156E-05
$\mu = 4$	-2.658E-08	9.155E-08	1.431E-07	1.454E-07	8.860E-08	-2.293E-07	-3.754E-07	-3.841E-07

Table 2.8 Full Annulus q =2.0, M_T =0.783

Upstream Waves, x=-b								
	m =16				m =-8			
	Real		Imag		Real		Imag	
	Namba	Schulten	Namba	Schulten	Namba	Schulten	Namba	Schulten
$\mu = 0$	-1.655E-04	-1.630E-04	-5.795E-05	-3.128E-05	8.854E-04	8.971E-04	-9.089E-05	-2.980E-04
$\mu = 1$	7.105E-06	6.334E-06	-1.076E-06	-3.142E-06	4.251E-03	3.284E-03	-2.294E-03	-1.984E-03
$\mu = 2$	-2.101E-06	-1.869E-06	9.234E-07	1.126E-06	-1.020E-06	-4.847E-05	-1.195E-04	-2.211E-04
$\mu = 3$	1.139E-06	1.113E-06	5.017E-07	5.386E-07	-2.845E-05	-2.699E-05	9.511E-06	8.071E-06
$\mu = 4$	1.707E-07	1.548E-07	-3.971E-07	-3.633E-07	4.429E-07	4.618E-07	2.714E-06	2.503E-06
Downstream Waves, x=+2b								
	m =16				m =-8			
	Real		Imag		Real		Imag	
	Namba	Schulten	Namba	Schulten	Namba	Schulten	Namba	Schulten
$\mu = 0$	-9.715E-06	-6.093E-06	-1.819E-05	-8.570E-06	1.026E-03	1.317E-03	3.203E-03	2.805E-03
$\mu = 1$	-8.477E-07	-2.302E-06	-3.636E-06	-4.420E-06	-4.846E-03	-5.003E-03	3.659E-03	4.453E-03
$\mu = 2$	-6.190E-07	-5.247E-07	-2.135E-07	-1.204E-07	1.139E-04	3.086E-05	-7.585E-05	-1.458E-04
$\mu = 3$	-1.372E-07	-8.094E-08	-6.714E-10	5.737E-08	5.670E-07	-5.327E-07	-3.561E-07	-1.646E-06
$\mu = 4$	-1.550E-08	-7.661E-09	-5.687E-10	8.106E-09	3.488E-08	1.104E-08	1.259E-08	-1.193E-08

Table 2.9 Full Annulus q =2.5, M_T =0.783

Upstream Waves, x=-b								
	m =16				m =-8			
	Real		Imag		Real		Imag	
	Namba	Schulten	Namba	Schulten	Namba	Schulten	Namba	Schulten
$\mu = 0$	1.120E-04	1.587E-04	8.099E-05	5.307E-05	-2.015E-03	-2.228E-03	2.092E-05	1.137E-03
$\mu = 1$	2.381E-06	-2.963E-06	-3.944E-06	-8.550E-06	-2.597E-03	-3.704E-03	-1.874E-03	1.704E-03
$\mu = 2$	3.718E-07	7.788E-07	3.257E-07	8.292E-07	1.562E-04	-2.159E-04	-4.155E-04	-6.501E-04
$\mu = 3$	-3.968E-07	-1.115E-07	4.161E-07	7.756E-07	6.050E-07	-5.117E-06	-5.274E-06	-1.060E-05
$\mu = 4$	2.676E-07	2.871E-07	9.914E-09	5.259E-08	-1.620E-06	-1.612E-06	9.243E-07	8.243E-07
Downstream Waves, x=+2b								
	m =16				m =-8			
	Real		Imag		Real		Imag	
	Namba	Schulten	Namba	Schulten	Namba	Schulten	Namba	Schulten
$\mu = 0$	3.383E-05	6.089E-05	4.788E-05	9.554E-06	-4.152E-04	-5.593E-04	-2.263E-03	-1.433E-03
$\mu = 1$	6.928E-07	-5.671E-06	-9.390E-06	-9.323E-06	-5.606E-03	-6.059E-03	-4.126E-04	3.095E-03
$\mu = 2$	-2.515E-07	2.610E-07	5.447E-07	5.622E-07	1.079E-04	-3.089E-04	-5.412E-04	-5.530E-04
$\mu = 3$	-9.519E-08	2.353E-07	4.061E-07	4.230E-07	1.625E-06	-5.251E-06	-8.799E-06	-9.154E-06
$\mu = 4$	-1.124E-08	3.304E-08	5.430E-08	5.849E-08	2.289E-08	-9.597E-08	-1.397E-07	-1.539E-07

Table 2.10 Full Annulus q =3.0, M_T =0.783

Upstream Waves, x=-b								
	m =16				m =-8			
	Real		Imag		Real		Imag	
	Namba	Schulten	Namba	Schulten	Namba	Schulten	Namba	Schulten
$\mu = 0$	-9.928E-05	-1.031E-04	-3.509E-05	-1.889E-05	5.764E-04	6.058E-04	-9.392E-05	-2.580E-04
$\mu = 1$	3.082E-06	2.825E-06	-3.724E-07	-1.612E-06	2.669E-03	2.213E-03	-1.441E-03	-1.365E-03
$\mu = 2$	-4.728E-07	-3.774E-07	6.002E-07	7.317E-07	-9.207E-06	-3.803E-05	-6.399E-05	-1.247E-04
$\mu = 3$	3.721E-07	3.761E-07	-2.232E-08	1.822E-08	-1.089E-05	-1.089E-05	3.008E-06	2.595E-06
$\mu = 4$	4.869E-08	5.559E-08	1.652E-08	1.860E-08	-4.233E-07	-4.470E-07	1.647E-07	1.683E-07

Downstream Waves, x=+2b								
	m =16				m =-8			
	Real		Imag		Real		Imag	
	Namba	Schulten	Namba	Schulten	Namba	Schulten	Namba	Schulten
$\mu = 0$	-5.613E-06	-3.755E-06	-1.069E-05	-4.942E-06	6.404E-04	8.712E-04	1.947E-03	1.768E-03
$\mu = 1$	-5.973E-07	-1.508E-06	-2.136E-06	-2.709E-06	-2.955E-03	-3.133E-03	2.274E-03	2.865E-03
$\mu = 2$	-3.657E-07	-3.265E-07	-1.472E-07	-9.456E-08	6.815E-05	2.212E-05	-4.114E-05	-8.419E-05
$\mu = 3$	-8.694E-08	-5.794E-08	-3.965E-09	3.026E-08	5.958E-07	-7.943E-09	-3.561E-07	-1.068E-06
$\mu = 4$	-9.828E-09	-6.417E-09	9.234E-11	4.465E-09	1.807E-08	8.769E-09	-1.317E-09	-1.267E-08

Table 3. Comparison of lift coefficient between 3D cascade (narrow annulus) at mid span and corresponding 2D cascade.

	3D (Narrow annulus)		2D	
M_T	Real	Imag	Real	Imag
0.3897	-2.263E-01	1.825E-01	-2.336E-01	1.971E-01
0.4330	-4.209E-02	1.064E-01	-4.030E-02	1.039E-01
0.4763	1.273E-02	1.453E-01	1.816E-02	1.413E-01
0.6495	8.959E-02	1.806E-01	9.709E-02	1.586E-01

Figures

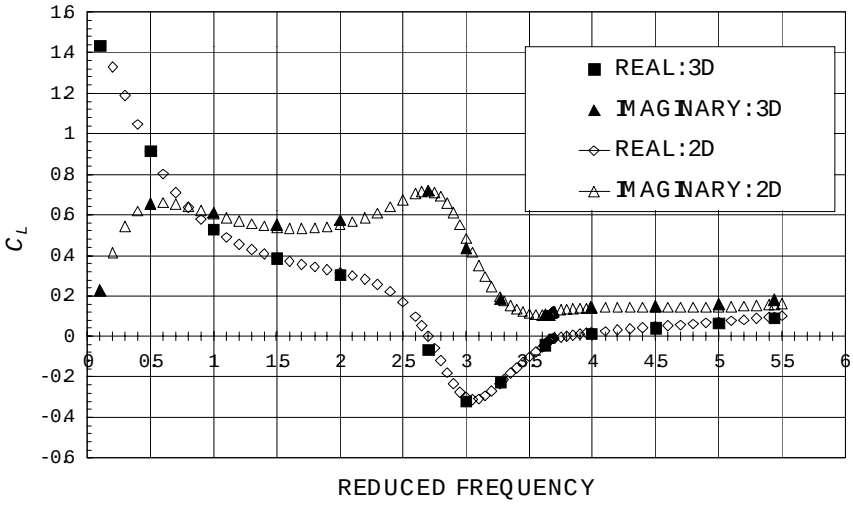

Figure 1 Comparison of lift coefficient between 3D cascade (narrow annulus) at mid span and corresponding 2D cascade. Reduced frequency =($2\pi B/V$)(M_T/M)

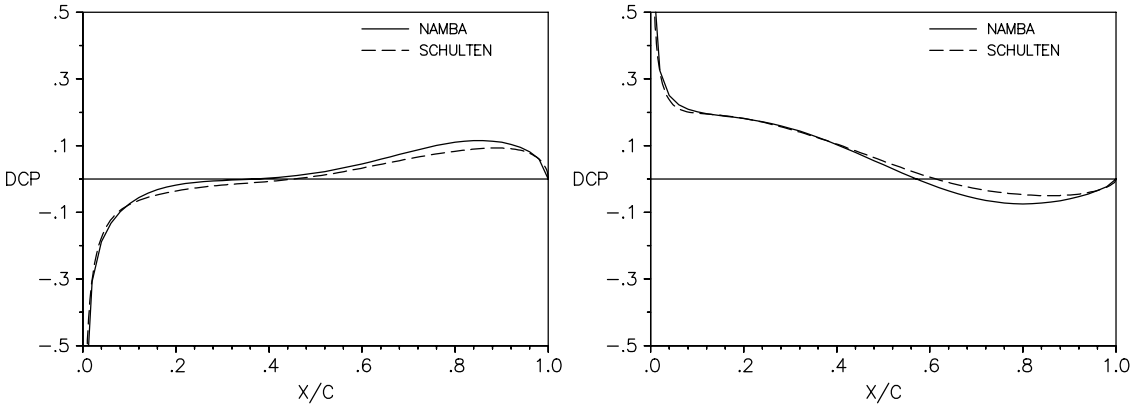

Figure 2 Real (left) and imaginary part of midspan ΔC_p, full annulus, q = 0, M_T = 0.783.

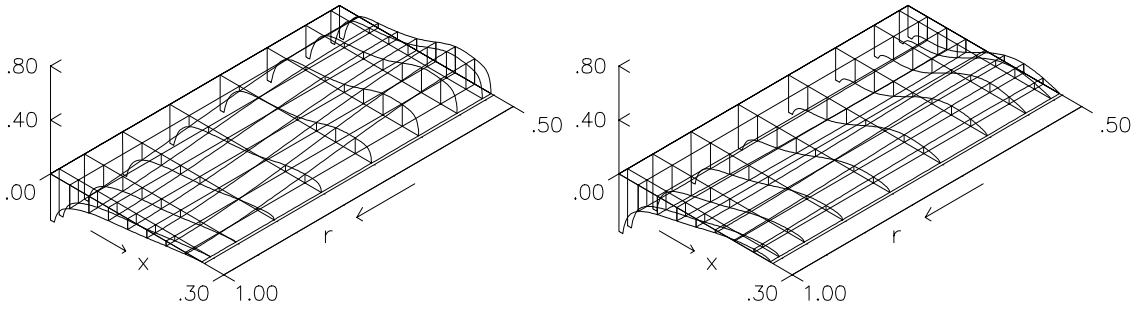

Figure 3 Real (left) and imaginary parts of ΔC_p, q = 0.0, M_T = 0.783

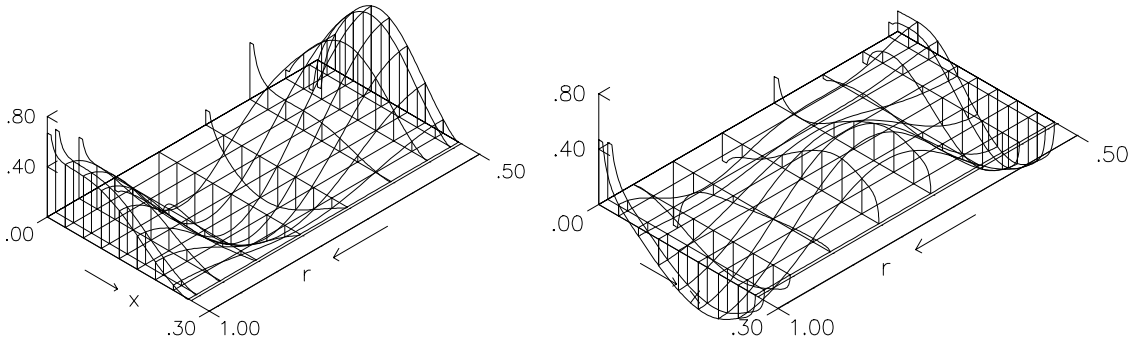

Figure 4 Real (left) and imaginary parts of ΔC_p, q = 1.5, M_T = 0.783

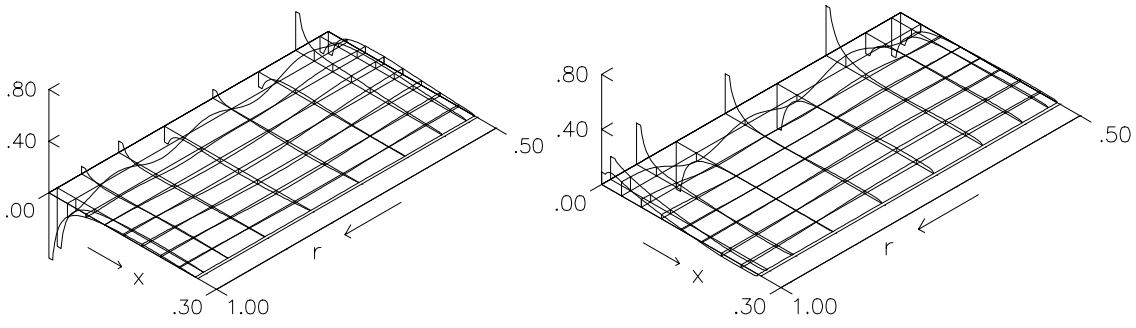

Figure 5 Real (left) and imaginary parts of ΔC_p, q = 3.0, M_T = 0.783

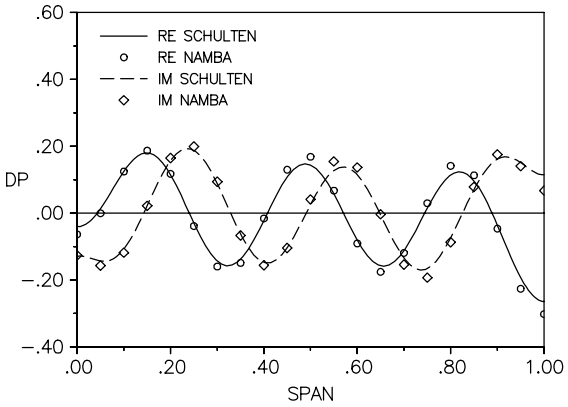

Figure 6 ΔC_p along x/c = 0.06, q = 3.0

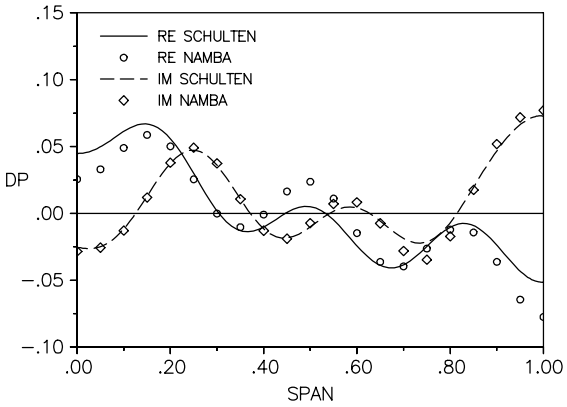

Figure 7 ΔC_p, along x/c = 0.2, q=3.0

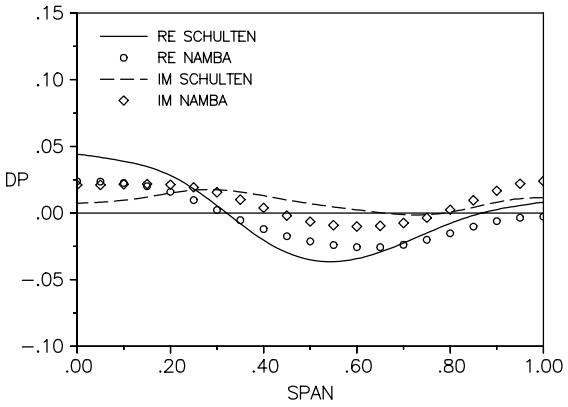

Figure 8 ΔC_p along x/c = 0.5, q = 3.0

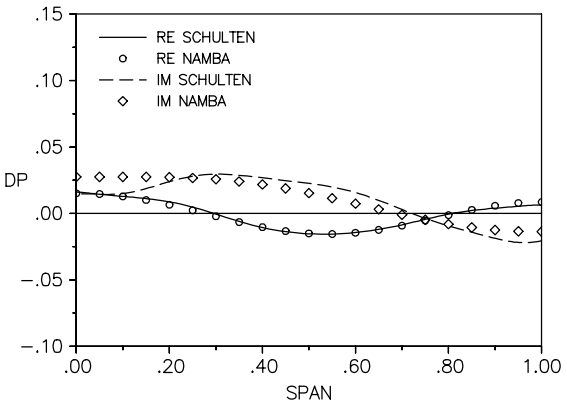

Figure 9 ΔC_p along x/c = 0.9, q = 3.0